Surface & Coatings Technology 326 (2017) 291–298

Contents lists available at ScienceDirect

Surface & Coatings Technology

journal homepage: www.elsevier.com/locate/surfcoat

Adhesion, tribological and corrosion properties of cold-sprayed CoCrMo and Ti6Al4V coatings on 6061-T651 Al alloy

Wen Sun [a,b], Adrian Wei Yee Tan [a,b], Iulian Marinescu [c], Wei Quan Toh [b], Erjia Liu [b,*]

[a] Rolls-Royce@NTU Corporate Lab, Nanyang Technological University, 50 Nanyang Avenue, Singapore 639798, Singapore
[b] School of Mechanical and Aerospace Engineering, Nanyang Technological University, 50 Nanyang Avenue, Singapore 639798, Singapore
[c] Advanced Technology Centre, Rolls-Royce Singapore Pte Ltd, Singapore

ARTICLE INFO

Article history:
Received 8 March 2017
Revised 12 July 2017
Accepted in revised form 27 July 2017
Available online 28 July 2017

Keywords:
CoCrMo coating
Ti6Al4V coating
Cold spray
Adhesion
Wear
Corrosion

ABSTRACT

In this study, CoCrMo and Ti6Al4V coatings were deposited on 6061-T651 aluminum alloy substrates via a high pressure cold spray process. Adhesion, tribological and corrosion properties of the CoCrMo and Ti6Al4V coatings were systematically investigated. The CoCrMo and Ti6Al4V coatings had good quality with low porosity levels and high hardnesses. X-ray diffraction patterns showed that there were no phase change and oxidation for the CoCrMo and Ti6Al4V coatings with reference to the CoCrMo and Ti6Al4V powder feedstocks. The shear bonding tests indicated good adhesion quality between the coatings and substrates. The tribological results showed that the CoCrMo coatings significantly enhanced the wear resistance of the Al alloy substrates. The corrosion results showed that the CoCrMo and Ti6Al4V coatings had higher anti-corrosion performances compared to the bare Al alloy substrates in a 3.5 wt% NaCl solution as the corrosion current densities for the CoCrMo and Ti6Al4V coated samples were substantially reduced.

1. Introduction

Aluminum alloys are widely used in aircraft, naval and building structural parts due to their low weight, good machinability and good ductility. 6061-T651 Al alloy is a kind of Al alloys, which contains Mg and Si as major elements. 6061-T651 Al alloy combines many good mechanical characteristics, such as moderately high strength, great machinability and good weldability, which make it a popular material for making aircraft parts (e.g. wings, fuselages and engine casings). However, when Al alloys are used in a high corrosive and wear environment, the surfaces of such materials will easily get corroded and worn.

CoCrMo alloys are widely used in various fields including aerospace industry to make cutlery, bearings, blades, etc. [1] where their high wear-resistance is needed. CoCrMo alloys are also capable of resisting oxidation and corrosive fumes and even boiling nitric acid [2].

Ti6Al4V is the most widely used alloy among all kinds of titanium alloys due to its low density, high strength and good resistance to corrosion in sea water, strong acid and alkali, which offers good chances for being used in aerospace and marine industries [3].

Al alloys can be easily distorted by heat, which requires a low temperature deposition technique to keep such alloy substrates at a low temperature during coating process. Traditional thermal spray methods use a torch to heat a material to a molten or near-molten state and use a gas to propel a coating material to the substrate surface, which induces much heat to the substrate. Cold gas dynamic spray, or "cold spray", is a newly developed surface coating technology [4], which can be employed in repair and additive manufacturing processes. Unlike thermal plasma spray or high velocity oxygen fuel spray (HVOF), cold spray does not use heat to bond powder particles to a substrate surface. As a consequence, both coatings and substrates are not influenced by oxidation, distortion or high-temperature thermal stress [5]. The microstructure of cold sprayed coatings can remain the same as the initial powder used for the deposition. For this reason, cold spray is a promising surface repair method for substrates or spray materials that are sensitive to heat or oxidation [6]. In a cold spray process, powder particles (ranging from 1 to 100 μm) are accelerated to a supersonic speed ranging from 500 to 1200 m/s. With high impact energies, the particles adhere to the substrate to form a dense coating [7].

Cold sprayed CoCrMo and Ti6Al4V coatings on 6061-T651 Al alloy substrates could provide an ideal solution for repairing the worn surfaces of Al alloy substrates as well as improving the wear and corrosion resistances of the substrates. By doing this, the favorable characteristics of 6061-T651 Al alloy and the good wear and corrosion resistances of CoCrMo and Ti6Al4V coatings can be ideally combined.

The interface bonding strength between coating and substrate is a crucial issue that should be considered when the quality of the coating is characterized [8]. Traditional methods to measure the adhesive strength of coatings are the pull-off tests, e.g. ASTM C633-13 [9], EN 582 [10] and ISO 14916 [11]. The limitation of these methods is that

* Corresponding author.
E-mail address: mejliu@ntu.edu.sg (E. Liu).

http://dx.doi.org/10.1016/j.surfcoat.2017.07.062
0257-8972/

appropriate adhesives must be used and the bonding strength of coating to substrate cannot be measured when its value is larger than the maximum glue strength. Wang et al. [12] measured the interfacial shear bond strength between cold sprayed 6061-T6 Al alloy coating and 6061-T6 Al alloy substrate, which was about 34.5 MPa. Xiong et al. [13] investigated the shear bond strength of Al 7075 coatings on the substrates of same material by using a lug shear test method, which showed that the shear bond strength increased from 8.7 MPa to 16.5 MPa with the coating thickness increased from 0.8 mm to 3.7 mm. Wang et al. [14] investigated the shear bond strength of cold sprayed composite coatings on AZ91 alloy substrates by using a specially designed lug shear method, which showed that the shear bond strength increased from 15 MPa to 35 MPa with the addition of Al_2O_3 in the coatings.

The tribological and corrosion performances of cold sprayed coatings have been studied by several researchers. Khun et al. [32] studied the wear and corrosion resistances of cold spayed Ti coatings, which showed that the wear resistance of Ti coatings performed better than Ti6Al4V substrates due to the work hardening of the cold sprayed Ti coatings. Astarita et al. [33] studied the wear properties of cold sprayed Ti coatings, which showed that laser treated Ti coatings performed better wear resistant properties compared to the Ti bulk. Khun et al. [34] studied the wear resistance of cold sprayed Ti6Al4V coatings by using He and N_2 as carrier gases, which showed that the Ti6Al4V coatings sprayed with He as the carrier gas had a better wear resistance. Khun et al. [34] also found that Ti6Al4V coatings sprayed with He as the carrier gas had lower anodic dissolution in a NaCl solution. Meydanoglu et al. [15] studied the corrosion performance of cold sprayed AA7075 matrix ceramic particles reinforced coatings, which showed that the AA7075 matrix composite coatings improved the anti-corrosion performance of the 6061-T6 Al substrates. Bandar et al. [16] investigated the corrosion performance of cold sprayed stainless steel 316L mixed with cobalt chromium coatings, which showed that the metal-metal mixture was more corrosion resistant than the pure stainless steel. However, there is no detailed study on the tribological and corrosion performances on CoCrMo and Ti6Al4V coatings deposited on 6061-T651 Al alloy substrates by utilizing a high pressure cold spray method.

This paper systemically studied the adhesion strength, wear resistance and anti-corrosion properties of cold sprayed CoCrMo and Ti6Al4V coatings on 6061-T651 Al alloy substrates. The shear bonding tests were carried out to characterize the coating adhesion strengths. The electrochemical and tribological measurements were conducted to investigate the wear and corrosion characteristics of the both uncoated and coated samples. The microstructure, surface topography, microhardness and phase composition were also systematically investigated.

2. Experimental details

2.1. Materials

The feedstock power materials used in this study were F75 CoCrMo (TLS Technik GmbH & Co. Spezialpulver KG, Germany) and Ti6Al4V Grade 23 (AP&C, Canada) powders with average particle sizes of 38 and 32 μm, respectively. Table 1 shows the particle size distributions of the CoCrMo and Ti6Al4V powders, where D10, D50 and D90 were defined as the particle sizes corresponding to cumulative size distribution at 10%, 50% and 90%, respectively [17]. The substrates used in this study were cut from a 5 mm-thick 6061-T651 Al alloy sheet that was provided by AMP, Singapore. Prior to cold spray deposition, the substrate surfaces were sand blasted [18] with fused alumina particles with a mean size of 80 μm at an angle of 45°. The angle 45° selected was to reduce the particle velocity and decrease the number of embedded particles [18]. The substrates were ultrasonically cleaned in an ethanol bath before cold spray deposition.

Table 1
Powder particle size distribution measured by using laser diffraction (ASTM B822-10) [19].

Cumulative fraction of particle size (%)	Powder particle size (μm)	
	CoCrMo	Ti6Al4V
D10	24.2	18.0
D50	38.4	31.6
D90	56.9	43.5

2.2. Cold spray deposition

A high pressure cold spray system (Impact Spray System 5/11, Impact Innovations GmbH, Germany) was used to perform the cold spray deposition, which consisted of a spray gun with a converging-diverging De Laval nozzle, two powder feeders, a gas control system and a water cooling system. A 160 mm long SiC nozzle with an inlet diameter of 13 mm, an outlet diameter of 6 mm and an expansion ratio of 5.6 was used to accelerate the particles to supersonic speed. The standoff distance between the nozzle exit and the substrate surface was 30 mm and the spray gun was vertical to the substrate surface. The nozzle scanning speed was fixed at 500 mm/s. The feed rates of the CoCrMo and Ti6Al4V powders were about 85 g/min and 40 g/min, respectively. The detailed cold spray process parameters were listed in Table 2. For the parameters used in this study, the average particle velocities of Ti6Al4V and CoCrMo powders were 800 m/s and 685 m/s, respectively, which were measured right before they impacted the substrate surfaces by using a cold spray velocimeter (ColdSprayMeter, Tecnar Automation Inc. St. Bruno. QC, Canada). In order to get 2 mm-thick coatings, the CoCrMo and Ti6Al4V coatings were deposited from 15 passes.

2.3. Characterization

After the cold spray deposition, the cross-sectional microstructures of the CoCrMo and Ti6Al4V coatings were analyzed by using optical microscopy (Zeiss Axioskop 2, USA). Prior to this process, the coated samples were mounted and polished by following the standard metallographic procedures. The porosity level of the coatings was analyzed by using the ImageJ software, which was guided by ASTM E2109-01. The images were captured with a magnification of 200× that allowed the voids in the coatings to be clearly resolved and the entire coating thickness properly displayed on the monitor screen. To calculate the porosity level, the optical images were converted into 32-bits black and white images. By adjusting the threshold function, the porosity levels of the coatings were determined.

The microhardnesses of the substrates and coatings were measured by using a Vickers hardness tester (Future-tech FM-300e, Japan) under the load of 500 g. The hardness measurements of the substrates were taken at the locations away from the coating-substrate interfaces. The microhardness values were averaged by taking ten measurements on each sample.

X-ray diffraction measurements were performed to analyze the phase compositions of the substrates, powders and coatings by using PANalytical Empyrean XRD equipment that used Cu Kα as the X-ray source. The scan speed was 1°/min with a scan step of 0.02° and the scan range was from 30° to 90°.

In this study, the interfacial bonding strength of the coated samples was measured by using shear lug test that was carried out by using a specially designed fixture shown in Fig. 1, which was compliant with the ČSN EN 15340 Standard [20]. The fixture was made to constrain the coating while the loading bar was applied onto the substrate. An

Table 2
Cold spray process parameters used in this study.

Propellant gas	Gas temperature	Gas pressure	Spray angle	Stand-off distance	Scan step
N_2	1000 °C	4.5 MPa	90°	30 mm	1 mm

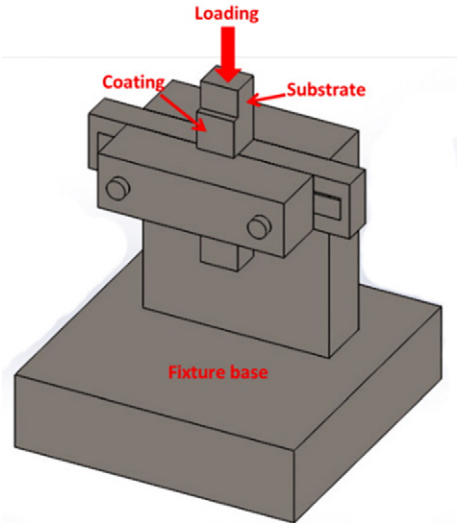

Fig. 1. Schematic diagram of lug shear test.

undercut of the substrate was also machined in order to ensure pure shear loading and minimal stress concentration due to the edge condition of the milling cutter used to prepare the samples [12]. The loading speed was 0.8 mm/s.

The friction and wear tests were conducted by using a ball-on-disk tribometer (CSM High Temperature Tribometer, USA), following the standard ASTM G99 [21]. The polished test sample surfaces were ultrasonically cleaned in the ethanol bath prior to the tribological tests. A 100Cr6 steel counter ball of 6 mm in diameter was used to slide on the rotating uncoated and coated sample surfaces along a circular path of 1.5 mm in radius for 20,000 laps at a sliding speed of 4 cm/s under a normal load of 1 N. The specific wear rate was calculated by using the formula below [32]:

$$\textit{Specific wear rate}\ (\mathrm{m^3/Nm}) = \frac{\textit{Wear Volume}\ (\mathrm{m^3})}{\textit{Normal load}\ (\mathrm{N}) \times \textit{Sliding distance}\ (\mathrm{m})}$$

The surface profiles as well as the wear tracks of the wear tested samples were measured by using a surface profilometer (Talyscan 150) with a diamond stylus of 4 μm, with an average specific wear rate from three measurements on each sample.

GAMRY (Interface 1000, USA) was used to measure potentiodynamic polarization curves. A flat cell kit (K0235, Princeton Applied Research) was set up with three electrodes, namely platinum counter electrode, Ag/AgCl reference electrode and working electrode (test sample). A 3.5 wt% NaCl solution was used for the corrosion tests. The polished test samples were ultrasonically cleaned in the ethanol bath prior to the corrosion testing. Open circuit potentials and potentiodynamic curves were measured on the coated and uncoated samples with a scan rate of 0.5 mV/s, from which the corrosion potential (E_{corr}) and corrosion current (i_{corr}) were determined. The i_{corr} values were calculated from the cathodic and anodic Tafel plots by using a Tafel extrapolation method [22,23].

3. Results and discussion

3.1. Morphologies of powders and coatings

Fig. 2a shows that the CoCrMo powder particles have a spherical shape with a mean size of 38 μm. In Fig. 2b, the EDX spectrum of the CoCrMo powder displays the Co, Cr and Mo peaks. Fig. 2c shows that the Ti6Al4V powder particles also have a spherical shape with a mean size of 32 μm. In Fig. 2d, the EDX spectrum of the Ti6Al4V powder displays the Ti, Al and V peaks.

Fig. 3 shows the surface morphologies of the as-deposited Ti6Al4V coating (Fig. 3a and b) and CoCrMo coating (Fig. 3c and d). It can be clearly seen that severe plastic deformations occur for the Ti6Al4V and CoCrMo particles due to high impact energies. At the same time, limited micropores and the particles with material jetting as compared with the original powders can be seen on the both CoCrMo and Ti6Al4V coating surfaces, which are also attributed to high particle impact energies. Fig. 3e and f shows that the surface roughnesses (Sa) of the as-sprayed Ti6Al4V and CoCrMo coatings are 15.8 ± 0.1 μm and 23.2 ± 0.2 μm, respectively.

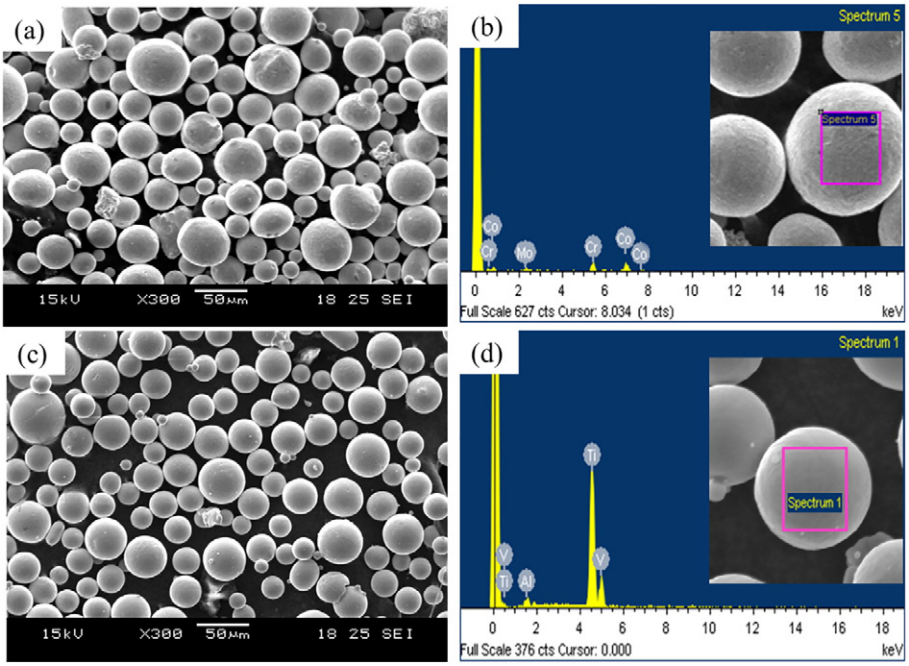

Fig. 2. (a & c) SEM micrographs showing (a) CoCrMo and (c) Ti6Al4V feedstock powders and (b & d) EDX spectra of (b) CoCrMo and (d) Ti6Al4V powders.

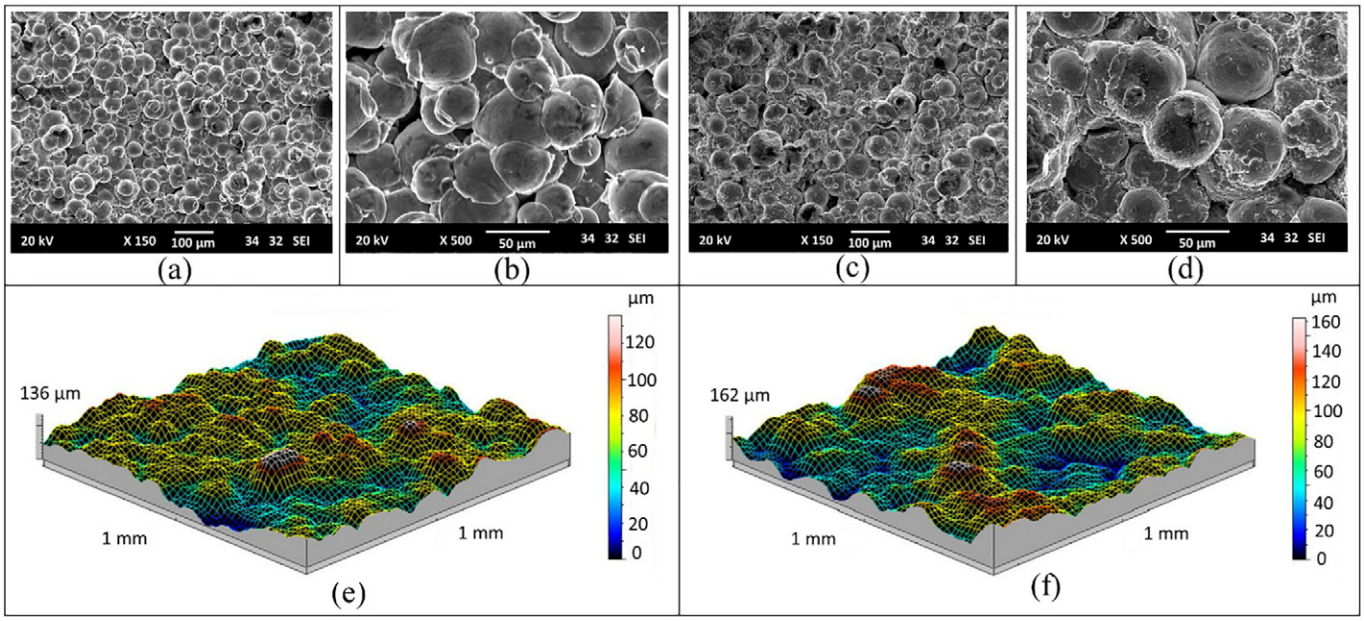

Fig. 3. (a–d) SEM micrographs showing the surface morphologies of (a & b) Ti6Al4V and (c & d) CoCrMo coatings at different magnifications and (e & f) surface profiles of (e) Ti6Al4V and (f) CoCrMo coatings.

3.2. Microstructure of Ti6Al4V and CoCrMo coatings

Fig. 4a shows the cross-sectional microstructure of the CoCrMo coating deposited from the first nozzle scan with a thickness of about 100 µm. It can be clearly seen that the CoCrMo particles are embedded into the Al alloy substrate because the softer substrate surface is plastically deformed by harder CoCrMo particles. No obvious plastic deformation of the CoCrMo particles is observed. This indicates that the physical trapping and mechanical interlocking have played an important role for the bonding of the CoCrMo coating to the Al alloy substrate [24].

However, the CoCrMo particles deposited from the second nozzle scan and onwards are deformed heavily and the bonding mechanisms are metallurgical bonding and mechanical interlocking due to physical deformation and adiabatic shearing instability [5]. The optical micrograph in Fig. 4b shows the cross-sectional microstructure of the CoCrMo coating with a thickness of about 2 mm. It can be seen that the CoCrMo coating is dense with only a few micropores and the local deformation of the CoCrMo particles is evident, which indicates that the cold sprayed CoCrMo coating is of superior quality. The porosity analysis results indicate that the porosity level of the cold-sprayed CoCrMo coatings is about 2.51 ± 0.20% that is much lower than that of flame-sprayed CoCrMo coatings (>10%) and plasma-sprayed CoCrMo coatings (5–8%) [25].

Fig. 4c and d shows the cross-sectional optical micrographs of the 2 mm-thick Ti6Al4V coating at different magnifications, which show

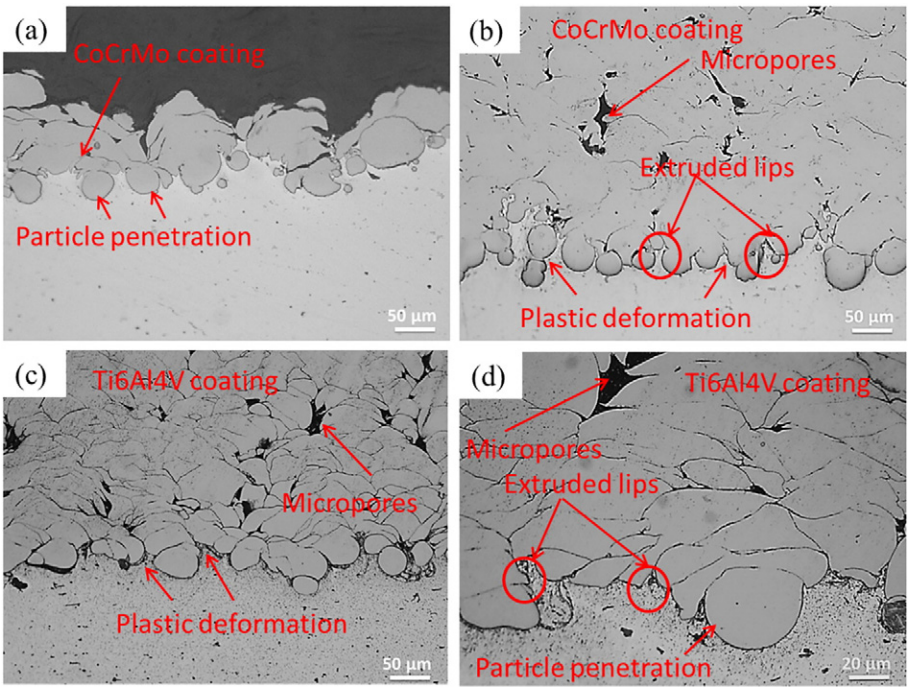

Fig. 4. Optical micrographs of (a & b) CoCrMo coatings on Al alloy substrates sprayed with (a) one pass of spraying and (b) 15 passes of spraying, and (c & d) a Ti6Al4V coating on Al alloy substrate at different magnifications.

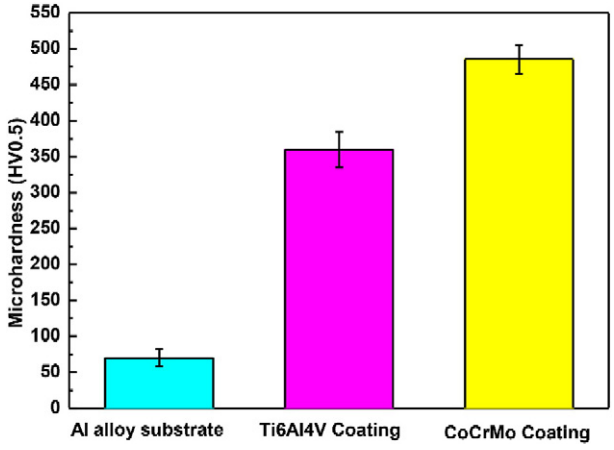

Fig. 5. Microhardnesses of Al alloy substrate and Ti6Al4V and CoCrMo coated samples.

the homogeneous Ti6Al4V coating with the coating/substrate interface being continuous and defect free. It is found that the deformation of the substrate is within about 30 μm from the coating/substrate interface. Below this depth, the substrate maintains its original microstructure. The Ti6Al4V particles penetrate into the substrate by mechanical interlocking. The porosity analysis results indicate that the porosity level of the cold-sprayed Ti6Al4V coating is about 2.83 ± 0.24%.

3.3. Microhardness

It is a common practice to qualify the coating process parameters and the extent of porosity in terms of coating microhardness [35]. Fig. 5 shows the microhardnesses of the uncoated Al alloy substrate and Ti6Al4V and CoCrMo coated samples with the average values of (70 ± 5) HV0.5, (362 ± 25) HV0.5 and (485 ± 20) HV0.5, respectively.

Table 3
Dimensions of coatings and their shear bonding strengths.

Coating type	Sample no.	Coating thickness (mm)	Coating surface area (mm^2)	Load (N)	Strength (MPa)	
					Measured	Average
CoCrMo coating	1	2.33	102.85	7081	68.85	66.17
	2	2.36	93.12	6077	65.26	
	3	2.40	145.59	9376	64.40	
Ti6Al4V coating	1	2.31	88.33	4603	52.11	50.38
	2	2.30	106.14	5328	50.20	
	3	2.35	107.25	5239	48.84	

The cold sprayed Ti6Al4V and CoCrMo coatings have tremendously improved the sample surface hardness. Due to the severe deformation of sprayed powder particles that takes place during the cold spray process, a complex strain hardening is expected, and nearly all the cold sprayed coatings tend to have a 20% to 40% higher hardness than their wrought counterparts [35]. The high hardnesses of the Ti6Al4V and CoCrMo coatings imply that the sprayed particles in the coatings are severely deformed thus leading to the dense coatings.

3.4. Phase analysis

Fig. 6a shows the XRD spectra of the Al alloy substrate before and after cold spray deposition. It can be clearly seen that there is no phase change in the substrate as the both spectra show the α-Al phase structure. Fig. 6b shows the XRD spectra of the CoCrMo powder feedstock and the cold sprayed CoCrMo coating, which show two phases, namely FCC (γ) and HCP (ε) chromium cobalt nickel molybdenum phases with the dominance of the γ phase over the ε phase. It has been reported that the presence of ε-phase is essential for the wear resistant properties of CoCrMo alloys [26] while γ phase is required for plasticity. There is no evidence that phase transition or oxidation occurs in the CoCrMo coatings during the cold spray deposition processes. The

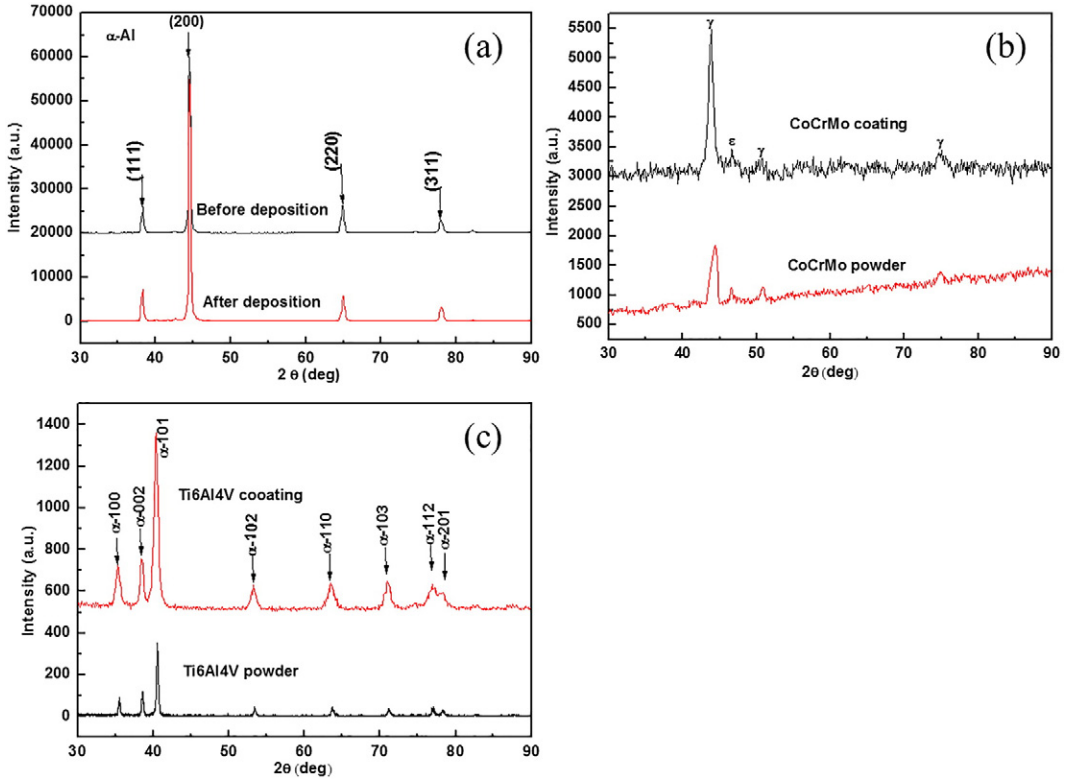

Fig. 6. XRD spectra of (a) Al alloy substrate before and after cold spray deposition, (b) CoCrMo powder feedstock and CoCrMo coating and (c) Ti6Al4V powder feedstock and Ti6Al4V coating.

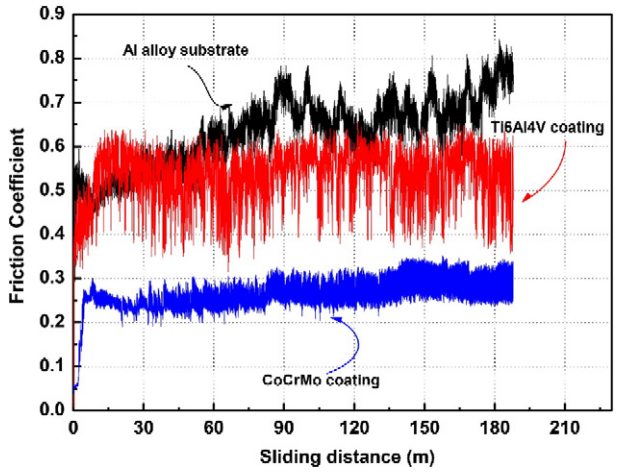

Fig. 7. Friction coefficients of Al alloy substrate and Ti6Al4V and CoCrMo coated samples.

broadened peaks for the CoCrMo coating indicate the severe plastic deformation of the embedded CoCrMo particles in the coating. Fig. 6c shows the XRD spectra of the Ti6Al4V powder feedstock and the sprayed Ti6Al4V coating, from which no apparent phase change can be observed in the coating as both the powder and the coating exhibit almost the same α phase structure [27]. No recognizable peaks corresponding to β phase can be found in the XRD spectra of the Ti6Al4V coating. The broadened peaks in the XRD spectra of the Ti6Al4V coating are due to the severe plastic deformation of the impacted Ti6Al4V particles in the coating during the cold spray process [27]. It should be noted that both the substrates and the powders have maintained their own original phase structures during the high pressure cold spray deposition processes.

3.5. Shear bonding test

The shear bonding test results measured at the coatings and substrate interfaces using the lug shear test are displayed in Table 3 with an averaged shear bonding strength from three measurements for each sample. Compared to the previous works reported by Wang et al. [12], Xiong et al. [13] and Wang et al. [14], the average shear bond strengths of the coated samples obtained in this study are obviously much higher. The higher shear bonding strengths of the CoCrMo and Ti6Al4V coatings are related to the higher densities of the cold sprayed coatings and the higher particle hardnesses. However, it is interesting to find that the average shear bonding strength between the CoCrMo coating and Al alloy substrate is around 66.17 MPa, which is higher than that between the Ti6Al4V coating and Al alloy substrate (around 50.38 MPa). The reason for this is probably because the CoCrMo particles have obtained a lot more momentum than the Ti6Al4V particles during cold spraying, which increases the impact energies of the CoCrMo particles. Although the velocities of the Ti6Al4V particles are higher than those of the CoCrMo particles, the density of CoCrMo powder material is around twice that of the Ti6Al4V powder. Thus, the impact energy of the CoCrMo particles is higher. From the microstructural images (Fig. 4), we can also see that the penetration of the sprayed CoCrMo particles into the substrate is deeper than that of the sprayed Ti6Al4V particles, which is in agreement with the shear bonding strength results.

3.6. Tribological behavior

Fig. 7 shows the friction coefficients of the Al alloy substrate and the cold-sprayed Ti6Al4V and CoCrMo coated samples with respect to the number of laps in the tribological tests. The fluctuations of the coefficients of friction are attributed to the alteration of real contact area, wear debris [28,33] and local contact temperature. The Al alloy substrate exhibits more severe fluctuations in coefficient of friction that is about 0.75 at the end of the test. The high fluctuations of coefficient of friction are probably because of the repeated formation and removal of oxide layer on the substrate surface and more severe wear of the substrate surface. The Ti6Al4V coated sample has a mean steady-state friction coefficient of about 0.60 with relatively large fluctuations too, which may be caused by the periodic formation and detachment of transfer layers on the surface as well as the variation of the local contact temperature [29]. The CoCrMo coated sample displays a more stable, much lower mean friction coefficient of about 0.25 at the steady state.

Fig. 8 shows the wear tracks of the Al alloy substrate and the Ti6Al4V and CoCrMo coated samples observed with surface profilometry after the wear tests. It can be clearly seen that the wear track of the substrate is wider and deeper than those of the Ti6Al4V and CoCrMo coated

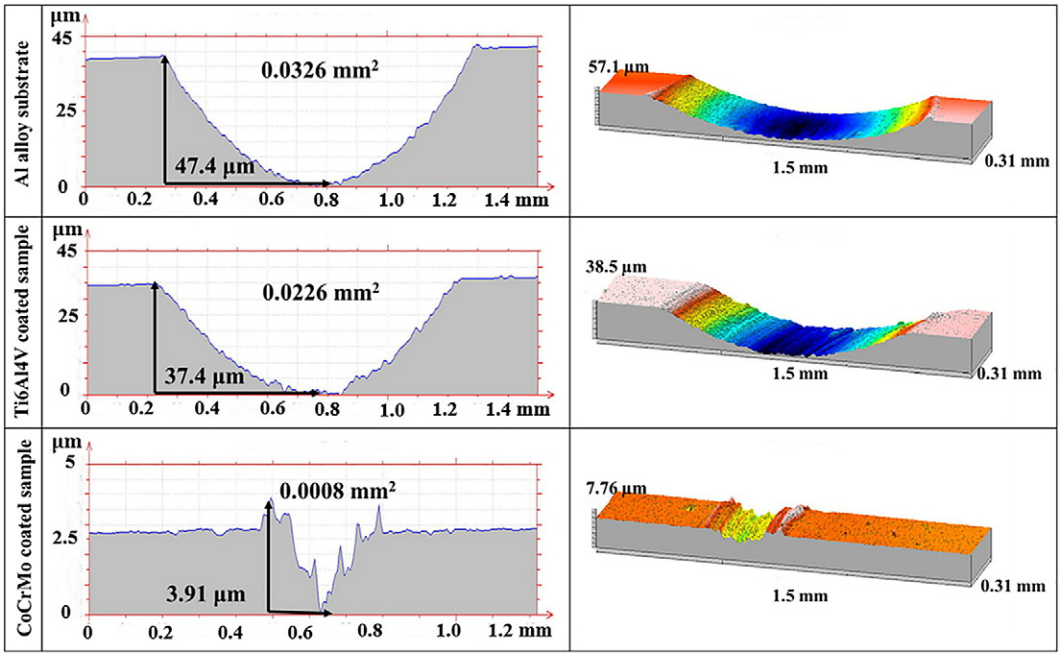

Fig. 8. Left: Cross-sectional profiles of wear tracks of uncoated and coated samples. Right: 3D surface profiles of corresponding wear tracks.

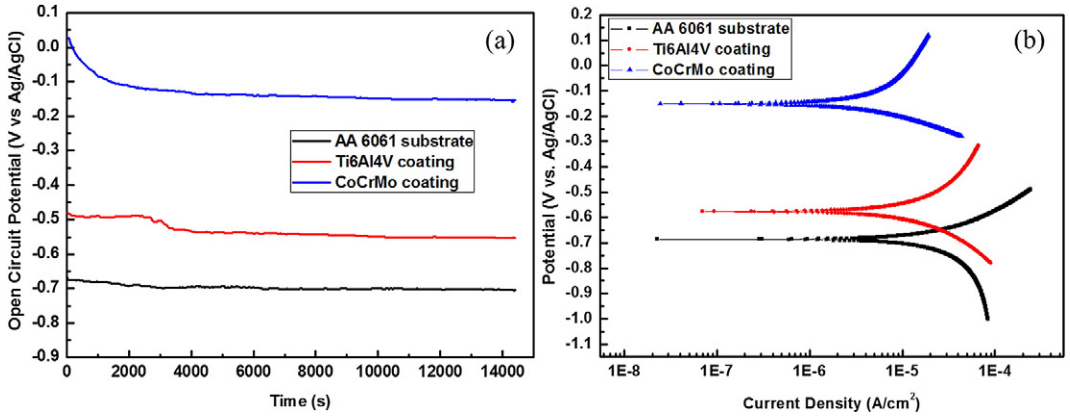

Fig. 9. (a) Open circuit potentials and (b) polarization curves of uncoated and Ti6Al4V and CoCrMo coated samples.

samples, which indicates the higher wear resistances of the CoCrMo and Ti6Al4V coatings. Through calculations, the specific wear rates of the Al alloy substrate and Ti6Al4V and CoCrMo coated samples are about 159 $\times 10^{-5}$ mm^3/Nm, 112 $\times 10^{-5}$ mm^3/Nm and 3.89 $\times 10^{-5}$ mm^3/Nm, respectively. The wear rate of the Ti6Al4V coating obtained in this study is consistent with the results reported by Khun et al. [34]. Compared to the CoCrMo coating, the lower wear resistance of the Ti6Al4V coating is due to the lower thermal conductivity of Ti6Al4V alloy [36]. During the rubbing process, the heat generated is dissipated slowly, which increases the interface temperature, thus deteriorating the tribological performance of the Ti6Al4V coating. The disruption of titanium dioxide (TiO_2) can also give rise to third-body wear [36]. Since the higher hardness of a solid material can lower its abrasive wear [34], the higher hardness of the CoCrMo coating can be correlated to its higher abrasive wear resistance. Meanwhile, the presence of ε-phase in the CoCrMo coating contributes to the improvement of the wear resistance of the CoCrMo coating [26]. The wear-resistance of the cold sprayed CoCrMo coatings is much higher than that of the Al alloy substrates in terms of specific wear rate, which indicates a good potential of the cold sprayed CoCrMo coatings for the wear protection of the Al alloy substrate surfaces.

3.7. Corrosion resistance

The corrosion behavior of the samples is analyzed by immersing the samples in a 3.5 wt% NaCl solution. The open circuit potentials (E_{ocp}) are measured during a 4 h immersion test (Fig. 9a), before the polarization curves are captured (Fig. 9b). The results of E_{ocp} show that the substrate presents a more active potential (lower E_{ocp}) than the Ti6Al4V and CoCrMo coated samples, indicating that the substrate surface is more susceptible to corrosion. It is also observed that the Ti6Al4V coated sample is more active than the CoCrMo coated sample. The stable OCP values of the samples suggest that stable oxide films may have already formed on their surfaces prior to exposure to the corrosion solution or in the early stage of exposure [37].

The potentiodynamic polarization curves of the coated and uncoated samples after the immersion tests are shown in Fig. 9b. The corrosion current density (i_{corr}) and corrosion potential (E_{corr}) values are determined from the polarization curves, which are summarized in Table 4. i_{corr} is directly related to corrosion rate, thus, reflecting the intensity of the constant corrosion process in a specific electrolyte [29],while E_{corr} is a measure of corrosion susceptibility [31]. It is observed that the E_{corr} of the CoCrMo and Ti6Al4V coated specimens is respectively 550 mV and 150 mV that are more positive compared to that of the uncoated Al alloy substrate. At the same time, the anodic current densities of the CoCrMo and Ti6Al4V coated specimens are much lower than that of the bare Al alloy substrate. The significantly higher E_{corr} and the substantially lower i_{corr} of the CoCrMo and Ti6Al4V coated specimens are attributed to their enhanced corrosion resistance compared to the bare substrate [30,31]. This improvement in corrosion resistance is more significant than that achieved by ceramic reinforced composite coatings in the case of the Al alloy [15].

Table 4
Results obtained from polarization curves and Tafel extrapolation.

Sample	E_{corr} (V)	i_{corr} (A/cm^2)
Al alloy substrate	−0.69	9.6E-05
Ti6Al4V coating	−0.54	4.5E-05
CoCrMo coating	−0.15	7.6E-06

4. Conclusions

In this study, CoCrMo and Ti6Al4V coatings were successfully coated on 6061-T651 Al alloy substrates via a high pressure cold spray process for the first time. The adhesion, tribological and corrosion characteristics of the CoCrMo and Ti6Al4V coatings were systematically investigated.

(1) The microstructural analysis showed that the porosity level of the CoCrMo and Ti6Al4V coatings was low and the coatings were strongly bonded to the substrates by physical trapping or mechanical interlocking. The sprayed CoCrMo and Ti6Al4V particles were severely deformed in the coatings, which implied that the velocities of the sprayed particles were well above their respective critical velocities during the cold spray processes.
(2) The average shear bonding strength between the CoCrMo coatings and Al alloy substrates was about 66.17 MPa, which was higher than that between the Ti6Al4V coatings and Al alloy substrates (about 50.38 MPa), due to the higher impact energies of the sprayed CoCrMo particles.
(3) The wear resistance of the CoCrMo coated samples was much higher than those of the bare Al alloy substrates and Ti6Al4V coated samples.
(4) The corrosion current densities of the CoCrMo and Ti6Al4V coated specimens were much lower than that of the uncoated Al alloy substrates. The significantly more positive shifts of the E_{corr} and the substantially lower i_{corr} values of the CoCrMo and Ti6Al4V coated specimens were attributed to the enhanced corrosion resistance of the CoCrMo and Ti6Al4V coatings.

Acknowledgments

This work was financially supported by the National Research Foundation (NRF), Rolls-Royce (RR), and Nanyang Technological University (NTU), Singapore, with the research grant number of NRF-RR-NTU M-RT3.1 Repair Technologies: Metal Cold Spray. Wen Sun was grateful for the PhD scholarship from the Rolls-Royce@NTU Corporate Lab and

the Nanyang Technological University, Singapore. Authors also thanked Anna Tai and Nicholas Weeks for their contributions to this work.

References

[1] B. Ratner, A. Hoffman, F. Schoen, J. Lemons, Biomaterial Science, 2nd edition Academic Press, 1996.
[2] E. Haynes, Metal alloy. US patent no. 873745, 1907.
[3] I. Inagaki, T. Takechi, Application and features of titanium for the aerospace industry, Steel & Sumitomo Metal Technical Report, 106, 2014, pp. 22–27.
[4] A.P. Alkhimov, V.F. Kosareve, A.N. Papyrin, A method of cold gas dynamic spray deposition, Dokl. Akad. Nauk SSSR 315 (1990) 1062–1065.
[5] H. Assadi, F. Gartner, T. Stolternhoff, H. Kreye, Bonding mechanism in cold gas spraying, Acta Mater. 51 (2003) 4379–4394.
[6] M.M. Sharma, T.J. Eden, B.T. Golesich, Effect of Surface Preparation on the Microstructure, Adhesion, and Tensile Properties of Cold-sprayed Al Coatings on AA2024 Substrates, 24, ASM International, 2014 410–422.
[7] V.F. Kosarev, S.V. Klinkov, A.P. Alkhimov, A.N. Papyrin, On some aspects of gas dynamics of the cold spray process, J. Therm. Spray Technol. 12 (2003) 265–281.
[8] M. St. Siegmann, H. Dvorak, K. Grützner, A. Walter Nassenstein, Shear testing for characterizing the adhesive and cohesive coating strength without the need of adhesives, Proceedings of ITSC 2005 Thermal Spray Connects: Explore Its Surfacing Potential! 2005, pp. 823–829.
[9] ASTM, C633, Standard Test Method for Adhesion or Cohesion Strength of Thermal Spray Coatings, 2013.
[10] EN 582, Thermal Spraying: Determination of Tensile Adhesive Strength, 1994.
[11] ISO 14916, Thermal Spraying: Determination of Tensile Adhesive Strength, 2015.
[12] X. Wang, F. Feng, M.A. Klecka, M.D. Mordasky, J.K. Garofano, T. El-Wardany, A. Nardi, V.K. Champagne, Characterization and modeling of the bonding process in cold spray additive manufacturing, Addit. Manuf. 8 (2015) 149–162.
[13] Y. Xiong, W. Zhuang, M. Zhang, Effect of the thickness of cold sprayed aluminium alloy coating on the adhesive bond strength with an aluminium alloy substrate, Surf. Coat. Technol. 270 (2015) 259–265.
[14] Q. Wang, K. Spencer, N. Birbilis, M. Zhang, The influence of ceramic particles on bond strength of cold spray composite coatings on AZ91 alloy substrate, Surf. Coat. Technol. 205 (2010) 50–56.
[15] O. Meydanoglu, B. Jodoin, E.S. Kayali, Microstructure, mechanical properties and corrosion performance of 7075 Al matrix ceramic particle reinforced composite coatings produced by the cold gas dynamic spraying process, Surf. Coat. Technol. 235 (2013) 108–116.
[16] B. Mangour, R. Mongrain, E. Irissou, S. Yue, Improving the strength and corrosion resistance of 316L stainless steel for biomedical applications using cold spray, Surf. Coat. Technol. 216 (2013) 297–307.
[17] Z. Sun, N. Ya, R.C. Adams, F.S. Fang, Particle size specifications for solid oral dosage forms: a regulatory perspective, Am. Pharmaceut. Rev. 13 (2010) 99–107.
[18] C.W. Ziemian, M.M. Sharma, B.D. Bouffard, T. Nissley, T.J. Eden, Effect of substrate surface roughening and cold spray coating on the fatigue life of AA2024 specimens, Mater. Des. 54 (2014) 212–221.
[19] ASTM: B822-10, Standard Test Method for Particle Size Distribution of Metal Powders and Related Compounds by Light Scattering, 2010.
[20] ČSN EN 15340, Thermal Spraying - Determination of Shear Load Resistance of Thermally Sprayed Coatings, 2007.
[21] ASTM G99, Standard Test Method for Wear Testing With a Pin-on-Disk Apparatus, 2016.
[22] S. Dehgahi, R. Amini, M. Alizadeh, Microstructure and corrosion resistance of Ni-Al_2O_3-SiC nanocomposite coatings produced by electrodeposition technique, J. Alloys Compd. 692 (2017) 622–628.
[23] L. Wang, J. Zhang, Z. Zeng, Y. Lin, L. Hu, Q. Xue, Fabrication of a nanocrystalline Ni-Co/CoO functionally graded layer with excellent electrochemical corrosion and tribological performance, Nanotechnology 17 (2006) 4614–4623.
[24] F. Meng, D. Hu, Y. Gao, S. Yue, J. Song, Cold-spray bonding mechanisms and deposition efficiency prediction for particle/substrate with distinct deformability, Mater. Des. 109 (2016) 503–510.
[25] P. Fauchais, A. Vardelle, Thermal Sprayed Coatings Used Against Corrosion and Corrosive Wear, Advanced Plasma Spray Applications, 51, 2012, pp. 1–10.
[26] D.H. Buckley, A.D. Sarker (Eds.), Wear of Metals, Pergamon Press, New York 1976, pp. 93–95.
[27] W. Sun, A.W.Y. Tan, N.W. Khun, I. Marinescu, E. Liu, Effect of substrate surface condition on fatigue behavior of cold sprayed Ti6Al4V coatings, Surf. Coat. Technol. 320 (2017) 452–457.
[28] G. Cassar, J.C.A.-B. Wilson, S. Banfield, J. Housden, A. Matthews, A. Leyland, A study of the reciprocating-sliding wear performance of plasma surface treated titanium alloy, Wear 269 (2010) 60–70.
[29] M. Mhaede, F. Pastorek, B. Hadzima, Influence of shot peening on corrosion properties of biocompatible magnesium alloy AZ31 coated by dicalcium phosphate dihydrate (DCPD), Mater Sci Eng C Mater Biol Appl 39 (2014) 330–335.
[30] R.K.S. Raman, S. Murray, M. Brandt, Laser assisted modification of surface microstructure for localised corrosion resistance of magnesium alloys, Surf. Eng. 2 (2007) 107–111.
[31] P.C. Banerjee, R.P. Woo, S.M. Grayson, A. Majumder, R.K.S. Raman, Influence of zeolite coating on the corrosion resistance of AZ91D magnesium alloy, Materials 7 (2014) 6092–6104.
[32] N.W. Khun, A.W.Y. Tan, E. Liu, Mechanical and tribological properties of cold-sprayed Ti coatings on Ti-6Al-4V substrates, J. Therm. Spray Technol. 25 (2016) 715–724.
[33] A. Astarita, F. Rubino, P. Carlone, A. Ruggiero, C. Leone, S. Genna, M. Merola, A. Squillace, On the improvement of AA2024 wear properties through the deposition of a cold-sprayed titanium coating, Metals 6 (2016) 1–12.
[34] N.W. Khun, A.W.Y. Tan, K.J.W. Bi, E. Liu, Effects of working gas on wear and corrosion resistances of cold sprayed Ti6Al4V coatings, Surf. Coat. Technol. 302 (2016) 1–12.
[35] C.M. Kay, J. Karthikeyan, High Pressure Cold Spray Principles and Applications, ASM International, 2016.
[36] S.R. Chauhan, K. Dass, Dry sliding behavior of titanium (Grade 5) alloy by using response surface methodology, Adv. Tribol. 1 (2013) 1–9.
[37] T. Marocco, T. Hussain, D.G. McCartney, P.H. Shipway, Corrosion performance of laser posttreated cold sprayed titanium coatings, J. Therm. Spray Technol. 20 (2011) 909–917.